DFT studies of fluorescence probe for selective detection of Zn^{2+} in the presence of Ca^{2+}, Mg^{2+}, Cu^{2+}, and Hg^{2+} ions

Krishanthi C. Weerasinghe[1,2] and Lichang Wang[1*]

[1]Department of Chemistry and Biochemistry, Southern Illinois University Carbondale, Carbondale, IL 62901, USA

[2]Department of Chemistry, Siena Heights University, Adrian, MI 49221, USA

Abstract

Fluorescence sensors are an important analytical tool for monitoring biologically relevant analytes. For instance, an anthracene based sensor was designed and characterized for the detection of Zn^{2+} in our previous studies. However, selective detection of such a sensor in the presence of other metal cations is a critically important factor for its practical application. In this work, we employed density functional theory calculations to study the selectivity of this anthracene sensor in the detection of Zn^{2+} in the presence of Ca^{2+}, Mg^{2+}, Cu^{2+}, and Hg^{2+} cations. DFT results indicate that the selectivity of the sensor on Zn^{2+} detection over the cations Ca^{2+}, Mg^{2+}, and Hg^{2+} is due to the binding selectivity as Zn^{2+} binds favorably to the sensor while Ca^{2+}, Mg^{2+}, and Hg^{2+} are no binding. Although Cu^{2+} binds to the sensor stronger than Zn^{2+}, the chelated sensor by Cu^{2+} reduces the UV-Vis absorption at the free sensor wavelength by 2 times and the fluorescence pathway is also not enhanced by the chelation, thus resulting response selectivity of Zn^{2+} over Cu^{2+}. Therefore, the present DFT study shows that the sensor selectivity on Zn^{2+} detection in the presence of Ca^{2+}, Mg^{2+}, Cu^{2+}, and Hg^{2+} is due to a combination of binding selectivity and response selectivity.

*Corresponding author: lwang@chem.siu.edu

1. Introduction

Organic small molecules have been widely studied as their importance in many applications, such as in sensing[1-41] and energy harvesting and conversion.[42-72] Over the last 30 years fluorescence has become the dominant detection and sensing technology in medical diagnostics and biotechnology.[25,73-76] Because of its ultra-high sensitivity, versatility, high speed of response, very high spatial resolution, non-destructive and non-invasive characters, fluorescence becomes a powerful technique for many biological and medical applications.[73,77,78]

In particular, Fluorescent sensors have become powerful tools for monitoring biologically relevant species in vitro and in vivo and to understand their functions.[74] Development of new sensors with good selectivity and sensitivity is a challenging and necessary task in 21st century. Among them fluorescence based sensors for metal ions have been of interest in recent years due to their importance in environmental monitoring by their ability to detect trace metal ions and also in medicinal field as powerful imaging agents.[75,79] These sensors are capable for detecting selective changes in fluorescence intensity and emission maxima upon binding to metal ions.[80]

Among the essential heavy metal ions in human body, Zn^{2+} is the second most abundant divalent cation in biological systems behind iron.[79,81-86] It is actively involved in various biological activities such as structural and catalytic cofactor of many proteins (e.g., carbonic anhydrase and zinc finger proteins) neural signal transmitters or modulators,[87] as a regulator of gene expression and cellular apoptosis.[85,86,88] Zn^{2+} is also known to have a role in neurological disorders, such as Parkinson's disease, Alzheimer's disease, amyotrophic lateral sclerosis, and epileptic seizures.[79,81] The detection of zinc ions is not only significant for the study of its biochemical functions, also important to quality control of food and nutrients for zinc supplements and assessment of environmental samples.[89] Some plants need higher concentration of zinc and grow only on zinc

contaminated soil. Furthermore, metal plating using zinc is the most important process to avoid corrosion of steel and plays a major role in material science.[86] In this regards, the development of fluorescent sensors for detection of zinc ions has become a very active area in the fields of biology and chemistry in recent years and some have been used successfully in zinc neurochemistry.[75] Development of fluorescent chemosensors for Zn^{2+} including small molecules, macromolecules and nanoparticals for the in vivo and in vitro detection of Zn^{2+} as well as with high selectivity over other metal ions have been successfully reported.[81,84,90-92] Most of them have been developed based on various fluorophores such as quinoline,[82,93,94] anthracene,[95] naphthalimide,[81,96] coumarin,[97] bodipy,[98] fluorescein,[99] rhodamine,[100,101] pyrene,[84,102,103] bipyridyl[104] and benzoxazole.[105] However, some of them usually require complicated synthesis involving severe reaction conditions and expensive chemicals. In addition, because of its closed-shell $3d^{10}4s^0$ electronic configuration and the absence of redox activity, the exact structural or functional roles, of Zn^{2+} in biological systems are not entirely clear.[106] Especially, lack of understanding of its mechanisms of action in comparison with other cations, such as, Na^+, K^+ and Ca^{2+}. As a consequence, there is considerable interest in detecting chelatable Zn^{2+} in biological systems.[81]

We have long been interested on detection of Zn^{2+} using PET mechanism. Previously, anthracene based PET sensor for the recognition of Zn^{2+} was reported using the computational predictions and the spectroscopic studies.[95] According to that, we reported the potential application of detection Zn^{2+} based on the preliminary spectroscopic studies and prediction from the gas phase calculations. In a later study, we designed and characterized another Zn^{2+} sensor using the same fluorophore and the receptor but, linked with a dimethylethanamine as a linker group.[107] Our calculations have shown that, the sensor has a favor binding selectivity to the Zn^{2+} over the Ca^{2+} ion. However, we haven't discussed the solvent effect and more importantly response selectivity

of Zn^{2+} over many biological cations (interfering cations). The abundant presence of transition metal cations may also due to their use in sensing[108-110] or catalysis in synthesis.[111-133] Therefore, in the present study we report the fluorescence response and selectivity of Zn^{2+} sensor over the competing cations such as Ca^{2+}, Mg^{2+} ,Cu^{2+} and Hg^{2+} using the previously discussed[95] anthracene based sensor in the solvent environment. We used anthracene as a fluorophore, pyridine as a receptor and an alkylamine bridge to synthesis the sensor. It is interesting to notice that, this sensor shows remarkable fluorescence enhancement after addition of Zn^{2+}. Such an increase in fluorescence efficiency can result from conformational restriction induced upon binding.[134,135] In additionally, it will enhance the molecular rigidity upon metal ion binding to chromophores with switch-on luminescence.[136-138] When the probe/sensor binds to its target, the rigidity of the probe–target duplex forces the stem to unwind, causing the separation of the fluorophore and the quencher and restoration of fluorescence. Further, theoretical methods such as Becke's three-parameter exchange functional with the Lee-Yang-Parr correlation functional (B3LYP)[82,95,107,139,140] and time dependent B3LYP (TD-B3LYP)[80,107,139,141] calculations provide further structural insights of this sensor.

2. Method

2.1 Computational Details

As we previously mentioned, the investigation of HOMO and LUMO levels of the isolated individual species are important to investigate whether these energy levels will be changed when the fluorophore and the receptor bind together. Therefore we have studied isolated fluorophore, isolated receptor, free sensor and the sensor bound with Zn^{2+}, Ca^{2+}, Mg^{2+},Cu^{2+}, and Hg^{2+}. All the structures were optimized at the DFT level using the GAUSSIAN09[142] package using B3LYP

exchange correlation functional.[80,95,107] B3LYP functional has been used to produce reliable results for such type of organic sensors and reported in many scientific publications.[80,107,143] All calculations of the above systems were performed using 6-311+G(d,p) basis set on the atoms of C, H, O, & N, and LanL2DZ[80,144,145] basis set for Zn, Ca, Mg, Cu, & Hg. Fully geometry optimizations were performed without any constraints. After the geometry optimization, to ensure the optimized geometry is a global minimum, frequency calculations were then conducted and checked for imaginary frequencies. The SCF convergence was 10^{-8} a.u and the gradient and energy conversion was 10^{-4} a.u and 10^{-5} a.u., respectively. We note that selected configurations were studied in the current work. Molecular dynamics simulations would be interesting in future studies to sample vast possible configuration space of binding.[146,147]

Excited state energies were calculated using Time Dependent Density Functional Theory (TDDFT) method.[80,107] Similar types of calculations were also performed with inclusion of solvent acetone for all the above systems using Polarizable Continuum Model (PCM). Six excited state energies were calculated for all the above mentioned TD-B3LYP calculations except Cu^{2+} bound system where we used twelve states. A detail explanation will be discussed when the excitation data are presented in section 3.

3. Results and Discussion

3.1. Comparison of Isolated Fluorophore and the Receptor with the Free Sensor

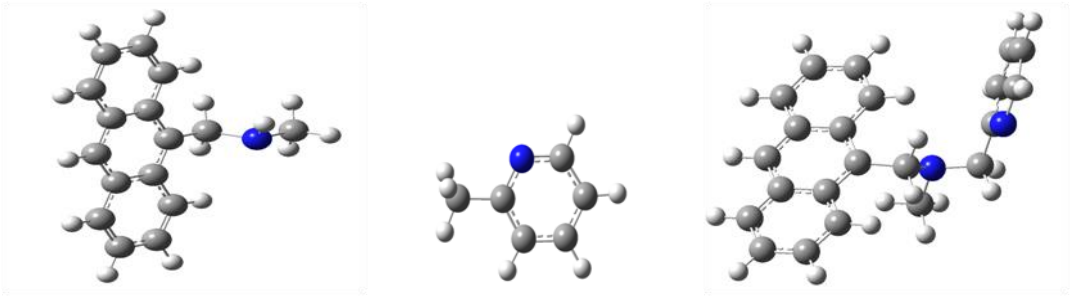

Figure 1. Optimized structures of isolated fluorophore [(anthracen-9-ylmethyl) methylmine], isolated receptor (2-methylpyridine) and the free sensor [(anthracen-9-ylmethyl)(benzyl)methylamine] using 6-311+G(d,p) basis set in acetone. The blue, gray and white balls represent nitrogen, carbon and hydrogen atoms respectively.

The optimized structure of isolated fluorophore, isolated receptor and the free sensor are shown in Figure 1. The first area of our analysis was based on the comparison of absorption spectra of the isolated fluorophore and the free sensor to observe the changes in absorption wavelengths when the receptor binds to the fluorophore. The simulated absorption spectra and calculated excitation energies are shown in Figure 2 and Table 1. As shown in Figure 2, the absorption bands were observed for both anthracene and free sensor in the range between 315-450 nm. It is interesting to notice that the absorption maximum of free sensor red shifted from 400 nm to 391 nm (~9 nm difference) when the pyridine receptor binds to the anthracene fluorophore. This is due to the spacer (alkyl amino group) between pyridine and the anthracene groups. It reveals that, there is no absorption band changes in the free sensor when the pyridine binds to the anthracene.

Table 1: Calculated Excitation Energies, and other Parameters of Isolated Fluorophore, receptor, and free sensor using 6-311+G(d,p)

Energy (eV)	Wavelength (nm)	Oscillator Strength	MOs	Coefficient
Fluorophore				
3.10	400	0.1084	H-2 → L+1	0.10451
			H → L	0.64472
3.52	354	0.0012	H-1 → L	0.69961
receptor				
5.29	234	0.0933	H-2 → L+1	0.30896
			H → L	0.62428
6.61	187	0.1279	H-1 → L+2	0.67341
			H-1 → L+4	0.11295
			H → L+1	0.10645
Free sensor				
3.08	402	0.1246	H-2 → L+3	0.10532
			H → L	0.64342
4.24	292	0.0077	H → L+2	0.68217
			H → L+3	0.13861

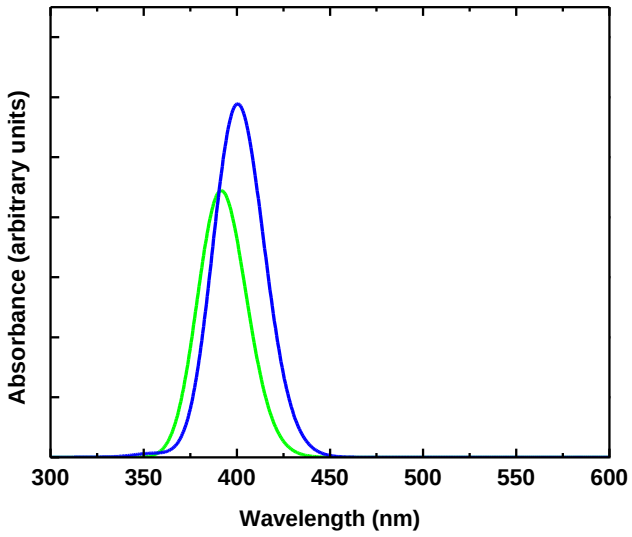

Figure 2. Absorption spectra for anthracene (blue) and free sensor (green).

It is important to mention that, we observed a calculated maximum absorption band for free sensor is 402 nm (Figure 3 and Table 1) which is consistent with the experimental results (388 nm). We note that the adsorption peaks in the region below 250 nm were not calculated in the fluorophore and free sensor studies.

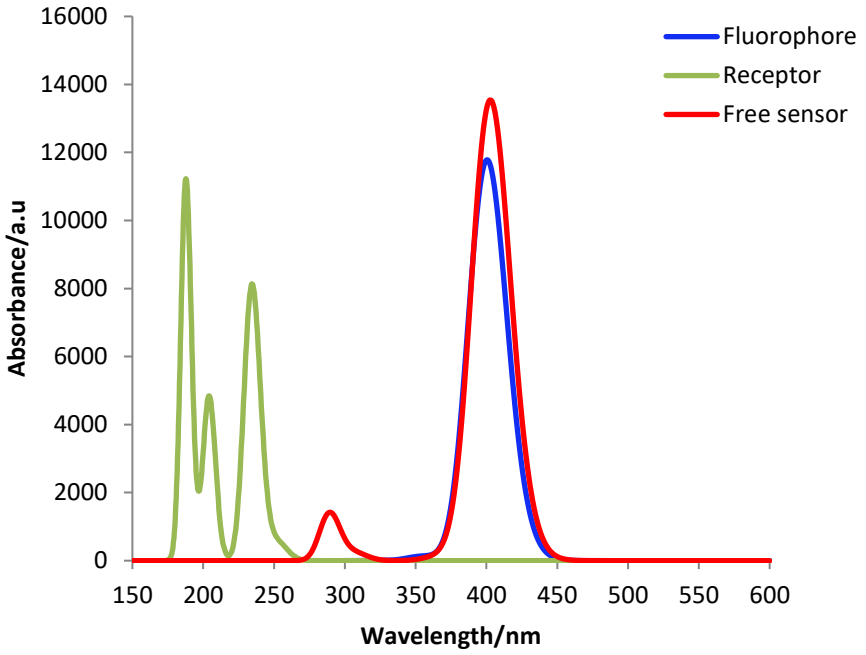

Figure 3.Calculated absorption spectra for fluorophore (blue), receptor (green) and free sensor (red) using 6-311+G(d,p) basis set in acetone.

The frontier molecular orbitals (MO) together with their energies corresponding isolated fluorophore, receptor and free sensor can be seen in Figure 4. Among the MOs in Figure 4, the majority of the electrons are confined with the anthracene moiety. When two isolated moieties coupled together to form a free sensor we expect fluorescence quenching. Based on the DFT and TDDFT calculated results shown in Figure 4 and Table S1, only ~10% of fluorescence signal can be quenched due to the electronic transition from H-2 to L+3 since L+1 and L+2 energy levels which are belong to the receptor. Since those are empty energy levels which can accept electrons from L+3 level and results in quenching the fluorescence signal. However, this may be due to

floppiness of the free sensor which could results in quenching via vibrational relaxations. Therefore a weak or "off" fluorescence state observed in the free sensor.

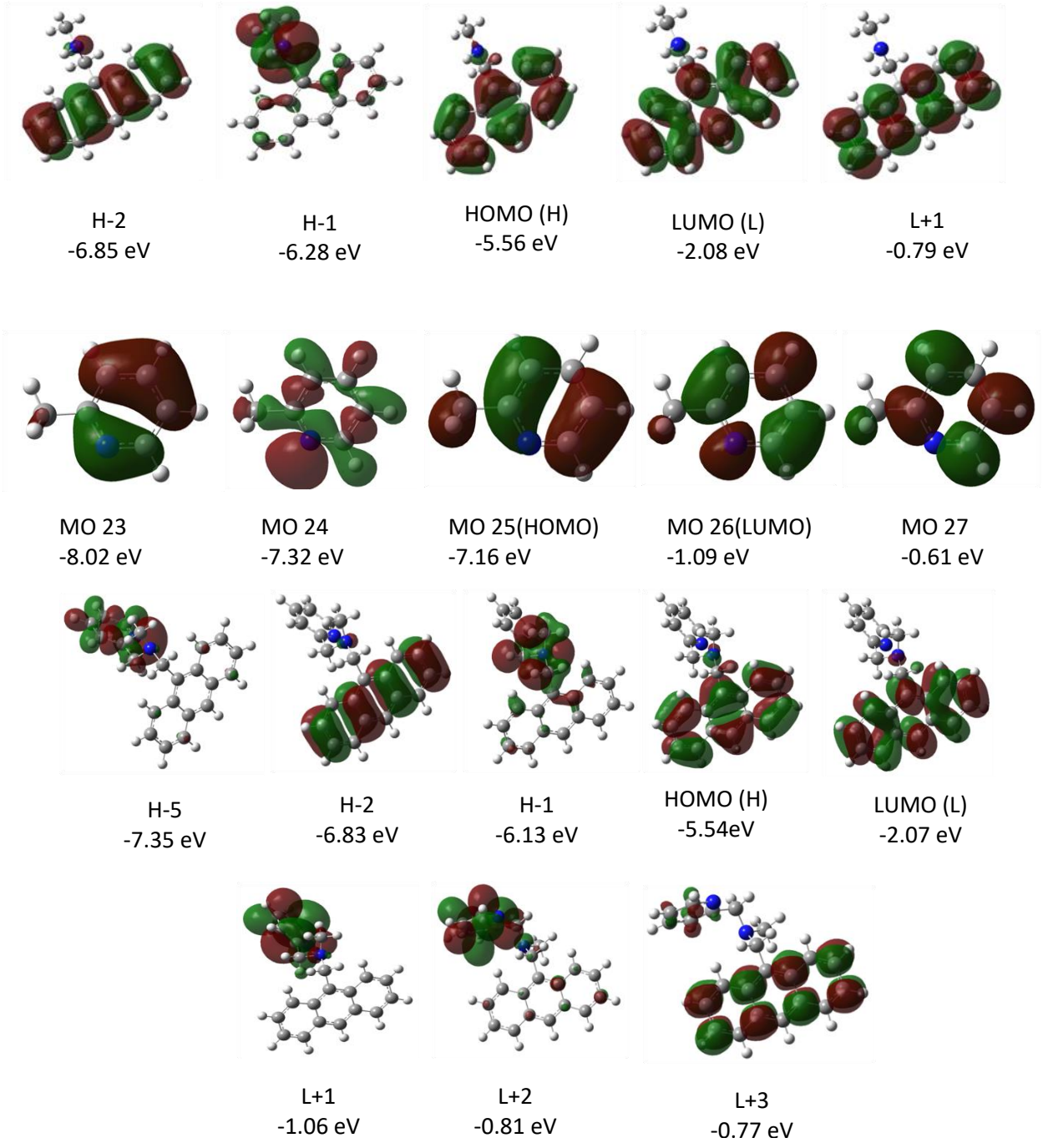

Figure 4. Energies and contours of MOs of isolated fluorophore (top), isolated receptor (middle), and free sensor (bottom two rows).

The energies and MOs corresponding to the free sensor are quite similar with the energies and the MOs of isolated fluorophore and the receptor. i.e. H-2, H, L and L+3 belong to the fluorophore while the H-5, L+1 and L+2 belong to receptor in terms of energy and the shape of the MO. The MO energy diagram can be depicted according to the MO energy levels obtained from each system separately which is shown in Figure 5. It is interesting to notice that, the difference in MO energies obtained from isolated components and the free sensor are almost negligible. This indicates that we can make direct comparisons among the MOs of isolated species and the free sensor.

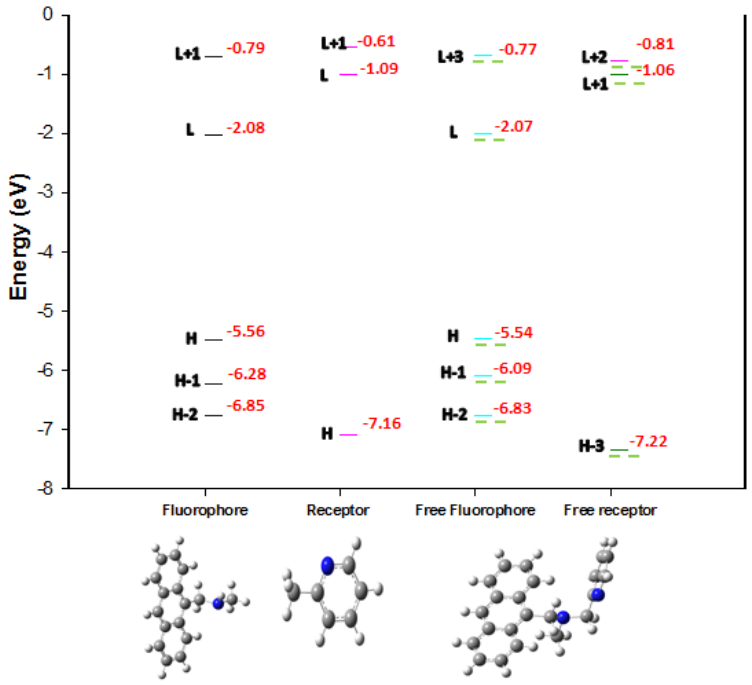

Figure 5. Energy diagram of isolated fluorophore, receptor and the free sensor. Green dash line represents energy levels of free sensor with the adding of a MeOH molecule.

Since the free sensor has a greater solubility in aprotic solvents, we expect introducing MeOH may results in formation of hydrogen bonding in the chelation site which can suppress the quenching response. We performed a DFT calculation for the free sensor by adding a MeOH molecule explicitly, (to form a hydrogen bond in acetone environment) to see the changes in energy levels. However, adding a MeOH molecule does not change energies significantly which are shown in green dash lines of depicted energy diagram in Figure 5. This confirmed that the hydrogen bonding do not play a significant role in this system. Therefore, we decided to use acetone as a solvent for further calculations to save CPU time.

3.2 Zn^{2+} Sensor

Upon binding with Zn^{2+} which is shown in Figure 6 undergoes dramatic structure changes. The receptor pyridine group tilled up to chelate with Zn^{2+} in order to form strong interactions between two N atoms. There is a two-coordination interaction with two N atoms (N in pyridine and methyl amine groups) and Zn^{2+} where the bond distances are 2.104˚A and 2.215˚A respectively. However, bond lengths are significantly larger than the typical sp^2 hybridized N and Zn bond length (~ 1.960 ˚A).[148] The dihedral angle between two N atoms (N1-C2-C3-N4) of free sensor is 117.58 while 33.73 for free sensor. Therefore these observations give clear evidence for the conformational changes of free senor upon addition of Zn^{2+} ions.

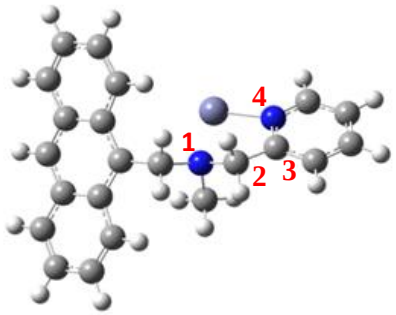

Figure 6. Optimized structure of Zn^{2+} bound sensor. The blue, gray, white, and gray-blue balls represent nitrogen, carbon, hydrogen, and zinc atoms respectively.

The calculated frontier molecular orbitals of Zn^{2+} bound sensor in acetone have been generated from the optimized structure and presented in Figure 6. It is interesting to notice that, most of the MOs, the electrons are mainly delocalized on the anthracene moiety such as H-2, H-1, H, L and L+2, but significant energy differences can be observed due to the Zn^{2+} interaction. The first three excitations of Zn^{2+} chelated sensor are illustrated in Table 2. Interestingly, the absorption band around 400 nm (~404 nm) was not change in the presence of Zn^{2+} which composed of HOMO to LUMO electronic transition. This peak is matched to that of isolated fluorophore/free sensor. In addition, there are two minor peaks which are at 368 nm, and 352 nm also appeared in our experimental absorption spectra (365 nm and 346 nm).

Table 2. Calculated Excitation Energies, and other Parameters of Zn^{2+} bound sensor using 6-311+G(d,p) and LanL2DZ Basis sets in Acetone

Energy (eV)	Wavelength (nm)	Oscillator Strength	MOs	Coefficient
3.05	404	0.1063	H → L	0.66067
3.37	368	0.0281	H → L+1	0.63771
			H → L+2	0.18750
3.52	352	0.0018	H → L+1	0.21956
			H → L+2	0.66758

The transition originated from H to L is more relevant to the fluorescence because, none of the receptor's MOs lie in between H and L of the Zn^{2+} bound sensor; i.e. this will hindered the electron transfer pathway and therefore restore the fluorescence. The titration plot shows that the fluorescence intensity increased up to ~32-fold upon increase of Zn^{2+} ions. This enhanced fluorescence could be due to the rigidity of Zn^{2+} bound sensor. During the titration, the emission intensity at 415 nm progressively increased with red shift (Δλ= 2nm). Such a change in emission is attributed to the better coordination of Zn^{2+} by amine N and pyridine N. Therefore, this will increase the rigidity of the molecule, and the photo-induced electron transfer from the binding site to excited state of anthracene is inhibited.

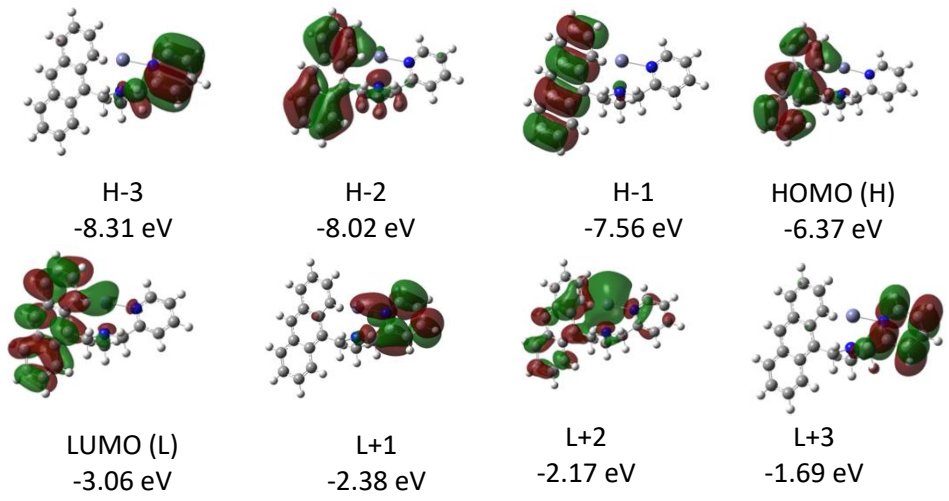

Figure 7. Energies and contours of MOs of Zn^{2+} bound sensor

Further, to confirm the fluorescence enhance is due to the rigidity of the sensor- Zn^{2+} complex we investigated the Raman spectra of anthracene, free sensor, and Zn^{2+} bound sensor as shown in Figure 8 and Figure 9. We focused the vibrational changes which are associated to anthracene fluorophore and alkyl amine bridge .The peaks appeared in between 3000-3160 cm^{-1} were due to the C-H stretching in the linker (bridge) group (middle figure). However this band was red shifted

when the free sensor is bonded to Zn^{2+} (2900-3120 cm^{-1}). The strong peak at 1423 cm^{-1} in the anthracene is due to the C=C stretching. This peak was blue shifted to 1432 cm^{-1} in the presence of pyridine receptor. However it reappeared in the same position as anthracene after the addition of Zn^{2+}. It indicates that the decrease rigidity of anthracene ring of the free sensor and the rigidity of sensor- Zn^{2+} complex. Also, the peak at 759 cm^{-1} in the anthracene red shifted to 711 cm^{-1} in the presence of Zn^{2+} due to the C=C stretching in the benzene rings at the two edges in the anthracene group. The peaks are attributed to the bending and rocking modes of the anthracene did not change, while most of the signals were weakened after the addition of Zn^{2+}.i.e. the peaks around 1200- 1550 cm^{-1} .Those observations gives clear evidence for the rigidity of anthracene molecule in the presence of Zn^{2+}. Therefore computational prediction matches with experimental data quite well. Furthermore, herein we report this sensor has a great selectivity towards physiologically active cations which we will discussed in next section.

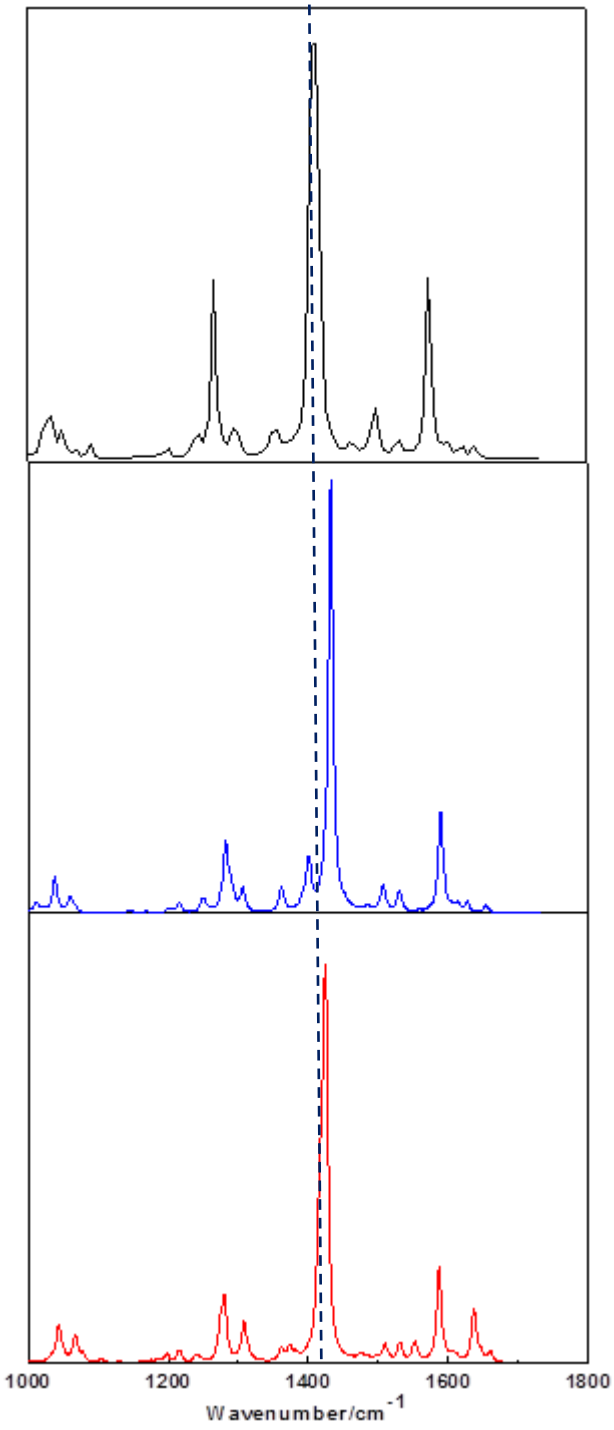

Figure 8. Raman spectra for anthracene (top), free sensor (middle) and Zn^{2+} bound sensor (bottom) using the B3LYP/6-311+G(d,p).

3.3 Selectivity of Zn^{2+} Sensor over Ca^{2+}, Mg^{2+}, Cu^{2+} and Hg^{2+} ions

One of the important aspects of many metal ion chelated sensors is their ability to detect specific metal ions over other competing metals ions (i.e. selectivity). Therefore, changes in the fluorescence intensity of free sensor caused by other metals ions, including Ca^{2+}, Mg^{2+}, Cu^{2+} and Hg^{2+} were important in developing sensor for selective detection of Zn^{2+}. To understand the fluorescence response of free sensor with each metal ions, we DFT calculations and the results of calculated binding energy (BE) of each metal bound sensor are shown in Table 3. It is interesting to notice that sensor binds with Zn^{2+} (-1.69 Kcal/mol) and Cu^{2+} (-6.93 Kcal/mol) but not with other metals, i.e. Ca^{2+} , Mg^{2+}, and Hg^{2+}, which have a positive BEs. This illustrate that the sensor has a binding selectivity towards Zn^{2+} in the presence of Ca^{2+} , Mg^{2+}, and Hg^{2+}. In the presence of Cu^{2+} ions, although it binds to the sensor, it is known to be strong fluorescence quencher via energy transfer or electron transfer pathways and therefore, the response from the presence of Cu^{2+} makes the sensor to be selective towards detection of Zn^{2+}.

Table 3: Energies of free sensor, bound sensors, metal cations and Binding energies of Zn^{2+}, Ca^{2+}, Mg^{2+}, and Cu^{2+} bound sensors using 6-311+g(d,p) + Lanl2DZ basis sets

Ion	Energy of free sensor/a.u	Energy of bound sensor/a.u	Energy of metal cation /a.u	Binding energy (Kcal/mol)
Zn^{2+}	-960.1342845	-1025.48578	-65.2892779	-1.69
Ca^{2+}	-	-996.303883	-36.42023437	6.82
Mg^{2+}	-	-960.5223471	-0.6058859	5.93
Cu^{2+}	-	-1155.978026	-195.5888292	-6.93
Hg^{2+}	-	-1002.375416	-42.4897283	6.76

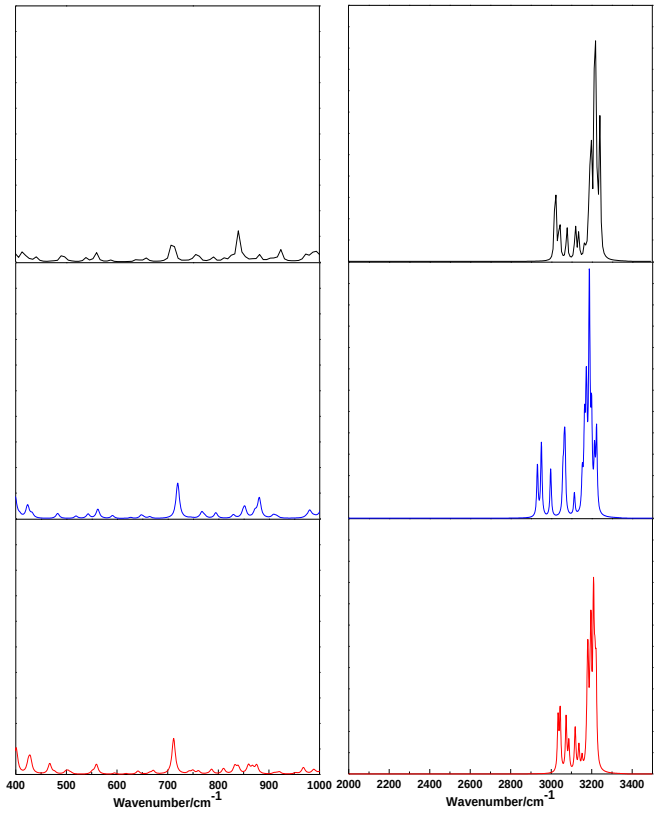

Figure 9. Raman spectra for anthracene (top), free sensor (middle) and Zn^{2+} bound sensor (bottom) using the B3LYP/6-311+G(d,p).

Table 4 provides the corresponding excitations (peaks have highest oscillator strengths) for each metal bound sensor in which includes excitation energy, wavelength, oscillator strength, MOs and the coefficients. The excitation at 389 nm of the Ca^{2+} bound senor with oscillator strength of 0.1413 is composed of two transitions, H-1 to L+3 and H to L. The one with highest determinant (0.64155) is more dominant and will produce fluorescent due to the absence of receptor MO in between H and L. More importantly, HOMO to LUMO transition is corresponding to fluorescence emission due to the absence of photo-induced electron transfer which is very similar to the Zn^{2+} bound sensor. The corresponding contours of MOs of Ca^{2+} bound sensor are shown in Figure 10.

Table 4. Calculated Excitation Energies, and other Parameters of Ca^{2+}, Mg^{2+}, Cu^{2+}, and Hg^{2+} Bound Sensor Using 6-311+G(d,p)+ Lanl2DZ Basis sets in Acetone

Ion	Energy (eV)	Wavelength (nm)	Oscillator Strength	MOs	Coefficient
Ca^{2+}	3.19	389	0.1413	H-1 → L+3	0.10416
				H → L	0.64155
Mg^{2+}	3.07	404	0.1211	H → L	0.64481
Cu^{2+}	2.98	416	0.0567	H-1 → L+1	0.17275
				H → L	0.11338
				H-10 → H	0.57076
				H-9 → H	0.41620
				H-8 → H	0.18231
				H-7 → H	0.25279
				H-6 → H	0.49895
Hg^{2+}	3.20	388	0.1392	H → L+1	0.69965

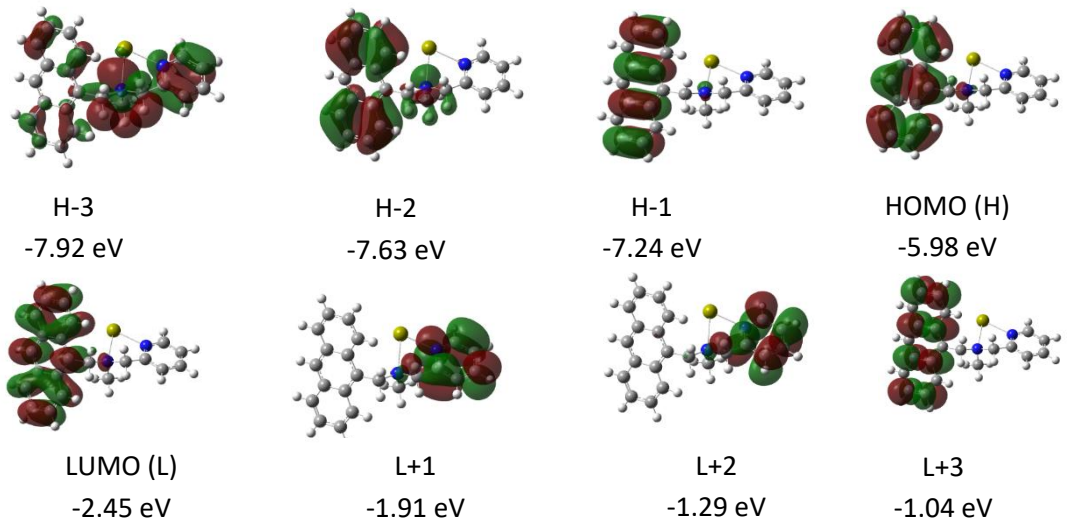

Figure 10. Energies and contours of MOs of Ca^{2+} bound sensor

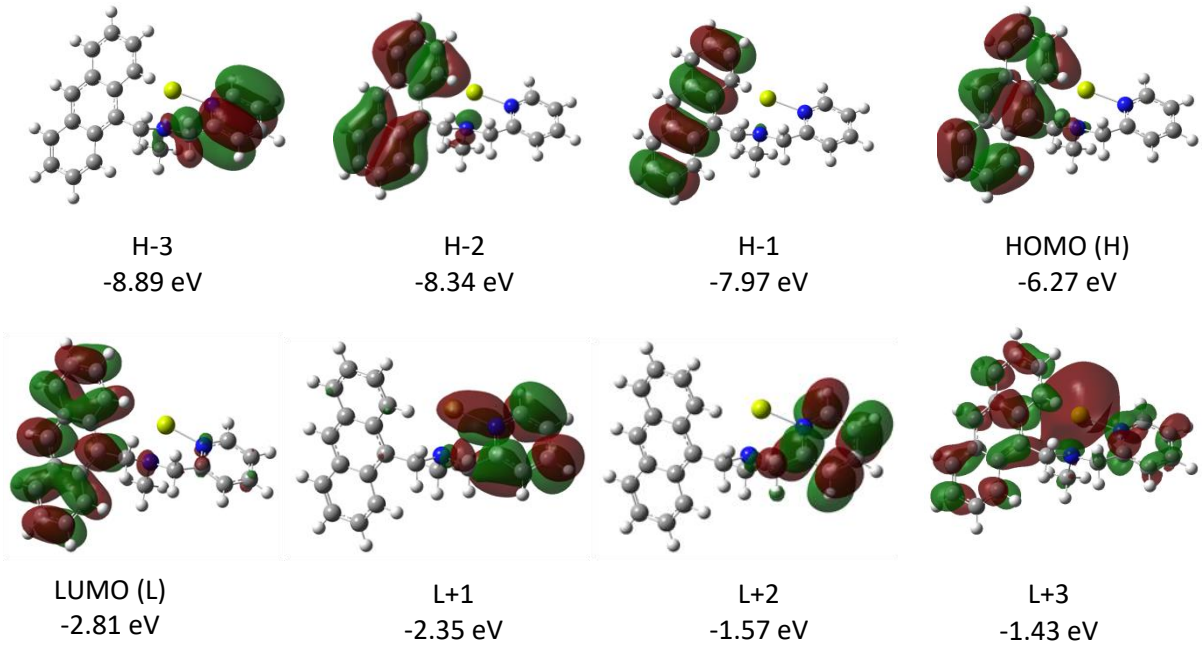

Figure 11. Energies and contours of MOs of Mg^{2+} bound sensor

In the presence of Mg^{2+} ions, the excitation wavelength at 404 nm was corresponding to HOMO to LUMO transition which will produce fluorescence emission. Similar prediction can be made for Hg^{2+} bound sensor as well. The transitions from H to L+1 will show a strong fluorescence emission because; L is localized in anthracene moiety which is an empty orbital. The corresponding contours of MOs of Mg^{2+} and Hg^{2+} bound sensors are shown in Figure 11 and Figure 12, respectively.

However, when Cu^{2+} ion bound to the sensor we observed an absorption band at 416 nm with the 0.0567 oscillator strength which was significantly lower in absorption intensity than the other metal bound sensors. Interestingly, this absorption peak corresponds to the several ETs and transition from H-10 to H is dominant due to the highest coefficient. Based on the contours of MOs and corresponding energies which are shown in Figure 13, three MOs: H-3, H-5 and H-6 belong

to the receptor moiety and while others belong to the anthracene. But, when the photo- excitation is taking place from H-10 to H the electron transfer/hole transfer can be taking place from low lying receptor MOs (H-3, H-5 and H-6) because they are occupied orbitals. Therefore, when the Cu^{2+} bound to the sensor it will hindered the fluorescence due to the photo-induced electron transfer process. Therefor we can argue that, although Cu^{2+} binds strongly (based on the large binding energy) it may be quenched rapidly via nonradioactive decay pathway.

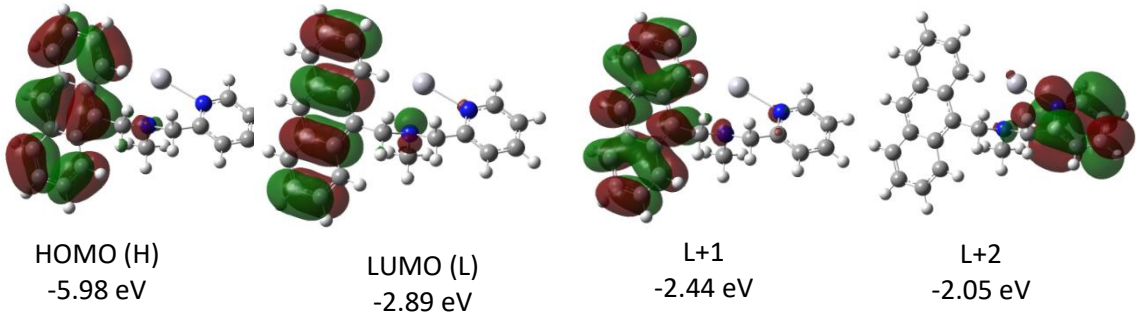

Figure 12. Energies and contours of MOs of Hg^{2+} bound sensor

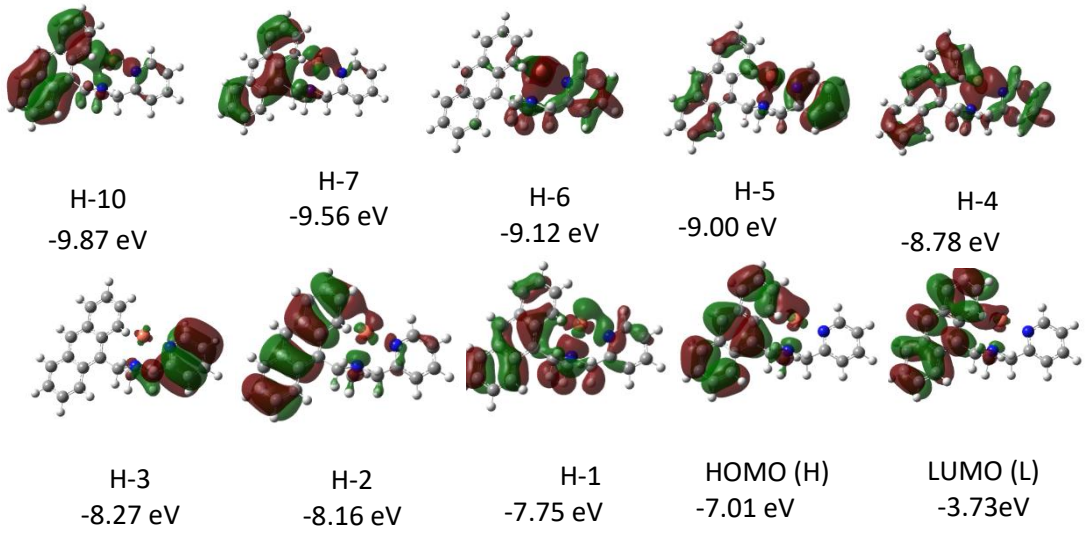

Figure 13. Energies and contours of MOs of Cu^{2+} bound sensor

4. Conclusions

In this work, we have carried out extensive DFT and TDDFT calculations to explore the selectivity of the anthracene based sensor on Zn^{2+} detection in the presence of other metal cations: Ca^{2+}, Mg^{2+}, Cu^{2+} and Hg^{2+}. In the case of free sensor, the fluorescence emission was quenched via non-radiative decay pathway, i.e. the sensor is at an off state and this is likely due to the floppiness of the free sensor. However, in the presence of Zn^{2+} cations, the fluorescence intensity of the sensor increases 65-fold over a 10-fold increase in Zn^{2+} concentration due to the inhibition of the electron-transfer partway. We previously speculated that this may be due to an enhanced rigidity of sensor-Zn^{2+} complex. This DFT study confirmed the rigidness through the calculated Raman spectra. The current DFT study also found that Zn^{2+} and Cu^{2+} bind to the sensor and other three cations, Ca^{2+}, Mg^{2+}, and Hg^{2+}, are no binding. Therefore, the selectivity of Zn^{2+} detection in the presence of Ca^{2+}, Mg^{2+}, and Hg^{2+} cations is due to binding selectivity. Although Cu^{2+} binds stronger than Zn^{2+}, it is known to be strong fluorescence quencher via energy transfer or electron transfer pathways. This is also observed in the calculated energy diagram. Therefore, this response selectivity between Zn^{2+} and Cu^{2+} allows selective detection of Zn^{2+} in the presence of Cu^{2+} cations. In summary, the current DFT study shows that the sensor selectivity on Zn^{2+} detection in the presence of Ca^{2+}, Mg^{2+}, Cu^{2+}, and Hg^{2+} cations is as a result of a combination of binding selectivity and response selectivity.

Acknowledgements

We thank Dr. Xiaoli Wang at SIUC for experimental insight into the sensor and Prof. Xin Xu from Fudan University for his advice on calculations during his visit to SIUC.

References

(1) Feng, W.; Zengji, Z.; Testoff, T. T.; Wang, T.; Yan, X.; Li, W.; Liu, D.; Wang, L.; Zhou, X. *Anal. Chim. Acta* **2021**, *1153*, 338278.

(2) Wang, T.; Liu, M.; Feng, W.; Cao, R.; Sun, Y.; Wang, L.; Liu, D.; Wang, Y.; Wang, T.; Hu, W. *Adv. Opt. Mater.* **2023**, 2202613.

(3) Liu, M.; Zong, J.; Wang, L.; Liu, D.; Wang, T.; Hu, W. *Adv. Opt. Mater.* **2022**, 2201684.

(4) Wang, T.; Liu, M.; Gao, C.; Song, Y.; Wang, L.; Liu, D.; Wang, T.; Hu, W. *Dyes Pigm.* **2022**, *207*, 110734.

(5) Liu, M.; Muleta, D. Y.; Yu, Z.; Wang, L.; Liu, D.; Wang, T.; Hu, W. *J. Mater. Chem. C* **2022**, *10*, 12249.

(6) Weerasinghe, K. C.; Wang, T.; Zhuang, J.; Liu, D.; Li, W.; Zhou, X.; Wang, L. *Comput. Mater. Sci.* **2017**, *126*, 244.

(7) Kumar, N. S.; Prasad, K. N. N.; Chandrasekhar, S.; Thipperudrappa, J. *Chem. Phys. Impact* **2023**, *6*, 100136.

(8) Zhao, M.; Wei, Q.; Zhang, J.; Li, W.; Wang, Z.; Du, S.; Xue, Q.; Xie, G.; Ge, Z. *Org. Electronics* **2022**, *100*, 106365.

(9) Zhao, J.; Zheng, X. *Front. Chem.* **2022**, *9*, 808957.

(10) Zhang, Y.; Mollick, S.; Tricarico, M.; Ye, J.; Sherman, D. A.; Tan, J.-C. *ACS Sens.* **2022**, *7*, 2338.

(11) Wang, Y.; Wang, X.; Ma, W.; Lu, R.; Zhou, W.; Gao, H. *Chemosensors* **2022**, *10*, 399.

(12) Li, J.; Dong, Y.; Wei, R.; Jiang, G.; Yao, C.; Lv, M.; Wu, Y.; Gardner, S. H.; Zhang, F.; Lucero, M. Y.; Huang, J.; Chen, H.; Ge, G.; Chan, J.; Chen, J.; Sun, H.; Luo, X.; Qian, X.; Yang, Y. *J. Am. Chem. Soc.* **2022**, *144*, 14351.

(13) Kuimov, A. D.; Becker, C. S.; Sonina, A. A.; Kazantsev, M. S. *New J. Chem.* **2022**, *46*, 21257.

(14) Khan, Q. U.; Begum, N.; Khan, K.; Rauf, M.; Zhan, Y. *Org. Electron.* **2022**, *103*, 106453.

(15) Geng, Y.; Zhang, G.; Chen, Y.; Peng, Y.; Wang, X.; Wang, Z. *Anal. Chem.* **2022**, *94*, 1813.

(16) Feng, Q.; Yang, T.; Ma, L.; Li, X.; Yuan, H.; Zhang, M.; Zhang, Y.; Fan, L. *ACS Appl. Mater. Interfaces* **2022**, *14*, 38594.

(17) Zhou, Q.; Xu, M.; Feng, W.; Li, F. *J. Phys. Chem. Lett.* **2021**, *12*, 9455.

(18) Zhou, Q.; Lei, Y.; Fu, H. *J. Mater. Chem. C* **2021**, *9*, 489.

(19) Zhai, C.; Yin, X.; Niu, S.; Yao, M.; Hu, S.; Dong, J.; Shang, Y.; Wang, Z.; Li, Q.; Sundqvist, B.; Liu, B. *Nat. Commun.* **2021**, *12*, 4084.

(20) Xie, Z.; Zhang, X.; Wang, H.; Huang, C.; Sun, H.; Dong, M.; Ji, L.; An, Z.; Yu, T.; Huang, W. *Nat. Commun.* **2021**, *12*, 3522.

(21) Wen, J.; Zhou, L.; Jiang, D.; Shan, X.; Wang, W.; Shiigi, H.; Chen, Z. *Anal. Chim. Acta* **2021**, *1180*, 338780.

(22) Tian, X.; Murfin, L. C.; Wu, L.; Lewis, S. E.; James, T. D. *Chem. Sci.* **2021**, *12*, 3406.

(23) Shin, Y.-H.; Gutierrez-Wing, M. T.; Choi, J.-W. *J. Electrochem. Soc.* **2021**, *168*, 017502.

(24) S., K.; Sam, B.; George, L.; N, S. Y.; Varghese, A. *J. Fluoresc.* **2021**, *31*, 1251.

(25) Price, J.; Balonova, B.; Blight, B. A.; Eisler, S. *Chem. Sci.* **2021**, *12*, 12092.

(26) Machnev, A.; Ofer, D.; Shishkin, I.; Kozlov, V.; Diaferia, C.; AntonellaAccardo; Morelli, G.; BorisApter; Inberg, A.; Rosenman, G.; PavelGinzburg *Sci. Rep.* **2021**, *11*, 17609.

(27) Liu, X.; Pan, Y.; Lei, Y.; Liu, N.; Dai, W.; Liu, M.; Cai, Z.; Wu, H.; Huang, X.; Dong, Y. *J. Phys. Chem. Lett.* **2021**, *12*, 7357−7364.

(28) Liang, N.; Zhao, Y. K.; Wu, Y. Z.; Zhang, C. R.; Shao, M. *Appl. Phys. Lett.* **2021**, *119*, 053301.

(29) Fang, T.; Elsen, F.; Vogeley, N.; Wang, D. *ACS Photonics* **2021**, *8*, 3448.

(30) Zhao, W.; He, Z.; Tang, B. Z. *Nat. Rev. Mater.* **2020**, *5*, 869.
(31) Pradeep, V. V.; Mitetelo, N.; Annadhasan, M.; Popov, M.; Mamonov, E.; Murzina, T.; Chandrasekar, R. *Adv. Opt. Mater.* **2020**, *8*, 1901317.
(32) Kiseleva, N.; Busko, D.; Richards, B. S.; Filatov, M. A.; Turshatov, A. *J. Phys. Chem. Lett.* **2020**, *11*, 6560.
(33) Grimm, J. B.; Tkachuk, A. N.; Xie, L.; Choi, H.; Mohar, B.; Falco, N.; Schaefer, K.; Patel, R.; Zheng, Q.; Liu, Z.; Lippincott-Schwartz, J.; Brown, T. A.; Lavis, L. D. *Nature Methods* **2020**, *17*, 815.
(34) Greiner, J.; Sundholm, D. *Phys. Chem. Chem. Phys.* **2020**, *22*, 2379.
(35) Alipour, M.; Damiri, S. *J. Chem. Phys.* **2020**, *152*, 204301.
(36) Wang, Q.; Jin, L.; Wang, W.; Hu, T.; Chen, C. *J. Lumine.* **2019**, *209*, 411.
(37) Strakova, K.; Assies, L.; Goujon, A.; Piazzolla, F.; Humeniuk, H. V.; Matile, S. *Chem. Rev.* **2019**, *119*, 10977.
(38) Han, J.; Feng, W.; Muleta, D. Y.; Bridgmohan, C. N.; Dang, Y.; Xie, G.; Zhang, H.; Zhou, X.; Li, W.; Wang, L.; Liu, D.; Dang, Y.; Wang, T.; Hu, W. *Adv. Funct. Mater.* **2019**, *29*, 1902503.
(39) Hwang, J. Y.; Lee, J.-Y.; Cho, C.-W.; Choi, W.; Lee, Y.; Shim, S.; Hwang, G. T. *Molecules* **2018**, *23*, 219.
(40) Zhang, X.-F.; Zhang, Y.; Liu, L. *J. Lumine.* **2014**, *145*, 448.
(41) Carter, K. P.; Young, A. M.; Palmer, A. E. *Chem. Rev.* **2014**, *114*, 4564.
(42) Xu, C.; Zhao, Z.; Yang, K.; Niu, L.; Ma, X.; Zhou, Z.; Zhang, X.; Zhang, F. *J. Mater. Chem. A* **2022**, *10*, 6291.
(43) Xu, F.; Gong, K.; Liu, D.; Wang, L.; Li, W.; Zhou, X. *Solar Energy* **2022**, *240*, 157.
(44) Weerasinghe, K. C.; Wang, T.; Zhuang, J.; Sun, H.; Liu, D.; Li, W.; Hu, W.; Zhou, X.; Wang, L. *Chem. Phys. Impact* **2022**, *4*, 100062.
(45) Gong, K.; Yang, J.; Testoff, T. T.; Li, W.; Wang, T.; Liu, D.; Zhou, X.; Wang, L. *Chem. Phys.* **2021**, *549*, 111256.
(46) Testoff, T. T.; Aikawa, T.; Tsung, E.; Lesko, E.; Wang, L. *Chem. Phys.* **2022**, *562*, 111641.
(47) Wang, R.; Gong, K.; Liu, R.; Liu, D.; Li, W.; Wang, L.; Zhou, X. *J. Porphyrins Phthalocyanines* **2022**, *26*, 469.
(48) Wang, T.; Weerasinghe, K. C.; Ubaldo, P. C.; Liu, D.; Li, W.; Zhou, X.; Wang, L. *Chem. Phys. Lett.* **2015**, *618*, 142.
(49) Xu, F.; Gong, K.; Fan, W.; Liu, D.; Li, W.; Wang, L.; Zhou, X. *ACS Appl. Energy Mater.* **2022**, *5*, 13780.
(50) Sun, H.; Liu, D.; Wang, T.; Li, P.; Bridgmohan, C. N.; Li, W.; Lu, T.; Hu, W.; Wang, L.; Zhou, X. *Org. Electronics* **2018**, *61*, 35.
(51) Wang, T.; Sun, H.; Zhang, L.; Colley, N. D.; Bridgmohan, C. N.; Liu, D.; Hu, W.; Li, W.; Zhou, X.; Wang, L. *Dyes Pigm.* **2017**, *139*, 601.
(52) Sun, H.; Liu, D.; Wang, T.; Lu, T.; Li, W.; Ren, S.; Hu, W.; Wang, L.; Zhou, X. *ACS Appl. Mater. Interfaces* **2017**, *9*, 9880.
(53) Wang, T.; Zhao, C.; Zhang, L.; Lu, T.; Sun, H.; Bridgmohan, C. N.; Weerasinghe, K. C.; Liu, D.; Hu, W.; Li, W.; Zhou, X.; Wang, L. *J. Phys. Chem. C* **2016**, *120*, 25263.
(54) Wang, T.; Weerasinghe, K. C.; Sun, H.; Hu, X.; Lu, T.; Liu, D.; Hu, W.; Li, W.; Zhou, X.; Wang, L. *J. Phys. Chem. C* **2016**, *120*, 11338.
(55) Wang, T.; Weerasinghe, K. C.; Liu, D.; Li, W.; Yan, X.; Zhou, X.; Wang, L. *J. Mater. Chem. C* **2014**, *2*, 5466.
(56) Yuan, B.; Zhuang, J.; Kirmess, K. M.; Bridgmohan, C. N.; Whalley, A. C.; Wang, L.; Plunkett, K. N. *J. Org. Chem.* **2016**, *81*, 8312.
(57) Zhou, X.; Liu, D.; Wang, T.; Hu, X.; Guo, J.; Weerasinghe, K. C.; Wang, L.; Li, W. *J. Photochem. Photobiol. A: Chem.* **2014**, *274*, 57.
(58) Xu, F.; Testoff, T. T.; Wang, L.; Zhou, X. *Molecules* **2020**, *25*, 4478.

(59) Zeng, L.; Huang, L.; Han, J.; Han, G. *Acc. Chem. Res.* **2022**, *55*, 2604.
(60) Yashwantrao, G.; Saha, S. *Dyes Pigm.* **2022**, *199*, 110093.
(61) Venkatesan, S.; Hsua, T.-H.; Wong, X.-W.; Teng, H.; Lee, Y.-L. *Chem. Eng. J.* **2022**, *446*, 137349.
(62) Liraz, D.; Tesslera, N. *Chem. Phys. Rev.* **2022**, *3*, 031305.
(63) Kousseff, C. J.; Halaksa, R.; Parr, Z. S.; Nielsen, C. B. *Chem. Rev.* **2022**, *122*, 4397.
(64) Koteshwar, D.; Prasanthkumar, S.; Singh, S. P.; Chowdhury, T. H.; Bedja, I.; Islam, A.; Giribabu, L. *Mater. Chem. Front.* **2022**, *6*, 580.
(65) He, S.; Lan, Z.; Zhang, B.; Gao, Y.; Shang, L.; Yue, G.; Chen, S.; Shen, Z.; Tan, F.; Wu, J. *ACS Appl. Mater. Interfaces* **2022**, *14*, 43576.
(66) Afraj, S. N.; Lin, C.-C.; Velusamy, A.; Cho, C.-H.; Liu, H.-Y.; Chen, J.; Lee, G.-H.; Fu, J.-C.; Ni, J.-S.; Tung, S.-H.; Yau, S.; Liu, C.-L.; Chen, M.-C.; Facchetti, A. *Adv. Funct. Mater.* **2022**, *32*, 2200880.
(67) Pujari, S. R.; Nagore, P. B.; Ghoti, A. J.; Mane, K. G. *J. Fluoresc.* **2021**, *31*, 259.
(68) Munoz-Garcia, A. B.; Benesperi, I.; Boschloo, G.; Concepcion, J. J.; Delcamp, J. H.; Gibson, E. A.; Meyer, G. J.; Pavone, M.; Pettersson, H.; Hagfeldt, A.; Freitag, M. *Chem. Soc. Rev.* **2021**, *50*, 12450.
(69) Kokkonen, M.; Talebi, P.; Zhou, J.; Asgari, S.; Soomro, S. A.; Elsehrawy, F.; Halme, J.; Ahmad, S.; Hagfeldt, A.; Hashmi, S. G. *J. Mater. Chem. A* **2021**, *9*, 10527.
(70) Whittemore, T. J.; Xue, C.; Huang, J.; Gallucci, J. C.; Turro, C. *Nat. Chem.* **2020**, *12*, 180.
(71) Carlotti, B.; Madu, I. K.; Kim, H.; Cai, Z.; Jiang, H.; Muthike, A. K.; Yu, L.; Zimmerman, P. M.; Goodson, T. *Chem. Sci.* **2020**, *11*, 8757.
(72) Zhou, R.; Jiang, Z.; Yang, C.; Yu, J.; Feng, J.; Adil, M. A.; Deng, D.; Zou, W.; Zhang, J.; Lu, K.; Ma, W.; Gao, F.; Wei, Z. *Nat. Commun.* **2019**, *10*, 5393.
(73) Demchenko, A. P. **2009**.
(74) Guo, Z.; Kim, G.-H.; Shin, I.; Yoon, J. *Biomaterials* **2012**, *33*, 7818.
(75) Sivaraman, G.; Anand, T.; Chellappa, D. *Analyst* **2012**, *137*, 5881.
(76) Markl, J. S.; Mueller, W. E. G.; Sereno, D.; Elkhooly, T. A.; Kokkinopoulou, M.; Garderes, J.; Depoix, F.; Wiens, M. *Biotechnol. Bioeng.* **2020**, *117*, 1789.
(77) Li, J.; Ballmer, S. G.; Gillis, E. P.; Fujii, S.; Schmidt, M. J.; Palazzolo, A. M. E.; Lehmann, J. W.; Morehouse, G. F.; Burke, M. D. *Science* **2015**, *347*, 1221.
(78) Chen, S.; Slattum, P.; Wang, C.; Zang, L. *Chem. Rev.* **2015**, *115*, 11967−11998.
(79) Hsieh, W. H.; Wanb, C.-F.; Liao, D.-J.; Wua, A.-T. *Tetrahedron Letters* **2012**, *53* 5848.
(80) Janaa, S.; Dalapatia, S.; Alamb, M. A.; Guchhait, N. *Journal of Photochemistry and Photobiology A: Chemistry* **2012** *238*, 7.
(81) Hanaoka, K.; Muramatsu, Y.; Urano, Y.; Terai, T.; Nagano, T. *Chem. Eur. J.* **2010**, *16*, 568
(82) Ramos, M. L.; Justino, L. L. G.; Branco, A.; Duarte, C. M. G.; Abreu, P. E.; Fonsecaa, S. M.; Burrowsa, H. D. *Dalton Trans.* **2011**, *40*, 11732.
(83) Lincoln, S. F. *Ausrealian Biochemist* **2004** *35*
(84) Zhang, Z.; Wang, F.-W.; Wang, S.-Q.; Ge, F.; Zhao, B.-X.; Miao, J.-Y. *Org. Biomol. Chem.* **2012**, *10*, 8640.
(85) Lin, H.-Y.; Cheng, P.-Y.; Wan, C.-F.; Wu, A.-T. *Analyst* **2012**, *137*, 4415.
(86) Ingale, S. A.; Seela, F. *J. Org. Chem.* **2012**, *J. Org. Chem.*, 9352−9356.
(87) Takeda, A. *BioMetals* **2001**, *14* 343.
(88) Kimura, E.; Aoki, S. *BioMetals 14* **2001**, 191.
(89) Maret, W. *BioMetals* **2001**, *14*, 187.
(90) Georgiev, N. I.; Lyulev, M. P.; Bojinov, V. B. *Spectrochimica Acta Part A: Molecular and Biomolecular Spectroscopy* **2012**, *97* 512.
(91) Ashokkumar, P.; Ramakrishnan, V. T.; Ramamurthy, P. *J. Phys. Chem. A* **2011**, *115*, 14292.
(92) Ciupa, A.; Mahon, M. F.; Bank, P. A. D.; Caggiano, L. *Org. Biomol. Chem.* **2012**, *10*, 8753.

(93) Mikata, Y.; Yamashita, A.; Kawata, K.; Konno, H.; Itami, S.; Yasudad, K.; Tamotsu, S. *Dalton Trans.* **2011**, *40*, 4059.
(94) Meng, X.; Wang, S.; Li, Y.; Zhu, M.; Guob, Q. *Chem. Commun.* **2012**, *48* 4196.
(95) McCarroll, M. E.; Shi, Y.; Harris, S.; Puli, S.; Kimaru, I.; Xu, R.; Wang, L.; Dyer, D. J. *J. Phys. Chem. B* **2006**, *110*, 22991.
(96) Jobe, K.; Brennan, C. H.; Motevalli, M.; Goldup, S. M.; Watkinson, M. *Chem. Commun.* **2011**, *47*, 6036.
(97) Xu, Z.; Liu, X.; Panb, J.; Spring, D. R. *Chem. Commun.* **2012**, *48*, 4764.
(98) Zhao, C.; Zhang, Y.; Feng, P.; Cao, J. *Dalton Trans.* **2012**, *41*, 831.
(99) Buccella, D.; Horowitz, J. A.; Lippard, S. J. *J. Am. Chem. Soc.* **2011**, *133*, 4101.
(100) Xu, L.; Xu, Y.; Zhu, W.; Zeng, B.; Yang, C.; Wu, B.; Qian, X. *Org. Biomol. Chem.* **2011**, *9*, 8284.
(101) Sasaki, H.; Hanaoka, K.; Urano, Y.; Terai, T.; Nagano, T. *Bioorganic & Medicinal Chemistry* **2011**, *19* 1072.
(102) Mei, Y.; Frederickson, C. J.; Giblin, L. J.; Weiss, J. H.; Bentley, Y. M. A. *Chem. Commun.* **2011**, *47*, 7107.
(103) Manandhar, E.; Broome, J. H.; Myrick, J.; Lagrone, W.; Cragg, P. J.; Wallace, a. K. J. *Chem. Commun.* **2011**, *47*, 8796.
(104) Sreenath, K.; Allen, J. R.; Davidson, M. W.; Zhu, L. *Chem. Commun.* **2011**, *47*, 11730.
(105) Xu, Y.; Pang, Y. *Dalton Trans.* **2011**, *40*, 1503.
(106) Zhang, Y.; Guo, X.; Jia, L.; Xu, S.; Xu, Z.; Zheng, L.; Qian, X. *Dalton Trans.* **2012**, *41*, 11776.
(107) Hudson, G. A.; Cheng, L.; Yu, J.; Yan, Y.; Dyer, D. J.; McCarroll, M. E.; Wang, a. L. *J. Phys. Chem. B* **2010**, *114*, 870.
(108) Cheng, H.-W.; Wu, Z.-P.; Yan, S.; Li, J.; Shan, S.; Wang, L.; Porter, M. D.; Zhong, C.-J. *Chem. Sci.* **2019**, *10* 7104.
(109) Jiang, W.; Xia, Y.; Pan, A.; Luo, Y.; Su, Y.; Zhao, S.; Wang, T.; Zhao, L. *Chemosensors* **2022**, *10*, 436.
(110) Qing, Z.; Bai, A.; Xing, S.; Zou, Z.; He, X.; Wang, K.; Yang, R. *Biosens. Bioelectron.* **2019**, *137*, 96.
(111) Ali, S.; Kumar, D.; Mondal, K. C.; El-Naas, M. H. *Catal. Commun.* **2022**, *172*, 106543.
(112) Wu, R.; Wang, L. *J. Phys. Chem. C* **2020**, *124*, 26953.
(113) Wu, R.; Wang, L. *Chem. Phys. Lett.* **2017**, *678*, 196.
(114) Xu, H.; Miao, B.; Zhang, M.; Chen, Y.; Wang, L. *Phys. Chem. Chem. Phys.* **2017**, *19*, 26210.
(115) Wu, Z.; Zhang, M.; Jiang, H.; Zhong, C.-J.; Chen, Y.; Wang, L. *Phys. Chem. Chem. Phys.* **2017**, *19*, 15444.
(116) Sun, K.; Zhang, M.; Wang, L. *Chem. Phys. Lett.* **2013**, *585*, 89.
(117) Wu, Z.-P.; Miao, B.; Hopkins, E.; Park, K.; Chen, Y.; Jiang, H.; Zhang, M.; Zhong, C.-J.; Wang, L. *J. Phys. Chem. C* **2019**, *123*, 20853.
(118) Miao, B.; Wu, Z.; Zhang, M.; Chen, Y.; Wang, L. *J. Phys. Chem. C* **2018**, *122*, 22448.
(119) Lu, J.; Aydin, C.; Browning, N. D.; Wang, L.; Gates, B. C. *Catal. Lett.* **2012**, *142*, 1445.
(120) Wang, L.; Williams, J. I.; Lin, T.; Zhong, C. J. *Catal. Today* **2011**, *165*, 150.
(121) Miao, B.; Wu, Z.-P.; Xu, H.; Zhang, M.; Chen, Y.; Wang, L. *Comput. Mater. Sci.* **2019**, *156*, 175.
(122) Miao, B.; Wu, Z.; Xu, H.; Zhang, M.; Chen, Y.; Wang, L. *Chem. Phys. Lett.* **2017**, *688*, 92.
(123) Wu, R.; Wang, L. *Chem. Phys. Impact* **2021**, *3*, 100040.
(124) Wu, C.; Wang, L.; Xiao, Z.; Li, G.; Wang, L. *Chem. Phys. Lett.* **2020**, *746*, 137229.
(125) Wu, R.; Wang, L. *Phys. Chem. Chem. Phys.* **2023**, *25*, 2190.
(126) Wu, R.; Wang, L. *J. Phys. Chem. C* **2022**, *126*, 21650.
(127) Wu, R.; Wang, L. *ChemPhysChem* **2022**, e202200132.
(128) Wu, C.; Wang, L.; Xiao, Z.; Li, G.; Wang, L. *Phys. Chem. Chem. Phys.* **2020**, *22*, 724.
(129) Fan, X.; Wu, Z.; Wang, L.; Wang, C. *Chem. Mater.* **2017**, *29*, 639.
(130) Qu, R.; Junge, K.; Beller, M. *Chem. Rev.* **2023**, *123*, 1103.

(131) Sarma, B. B.; Maurer, F.; Doronkin, D. E.; Grunwaldt, J.-D. *Chem. Rev.* **2023**, *123*, 379.
(132) Halawy, S. A.; Osman, A. I.; Rooney, D. W. *Energy Sci. Eng.* **2022**, *10*, 2827.
(133) Zhang, Z.; Chen, X.; Kang, J.; Yu, Z.; Tian, J.; Gong, Z.; Jia, A.; You, R.; Qian, K.; He, S.; Teng, B.; Cui, Y.; Wang, Y.; Zhang, W.; Huang, W. *Nat. Commun.* **2021**, *12*, 4331.
(134) McFarland, S. A.; Finney, N. S. *Journal of the American Chemical Society* **2002**, *124*, 1178.
(135) McFarland, S. A.; Finney, N. S. *Journal of the American Chemical Society* **2001**, *123*, 1260.
(136) Li, Y.; Shi, L.; Qin, L.-X.; Qu, L.-L.; Jing, C.; Lan, M.; Jamesb, T. D.; Long, Y.-T. *Chem. Commun.* **2011**, *47*, 4361.
(137) Ghosh, K.; Saha, I. *Tetrahedron Letters* **2010**, *51*, 4995.
(138) Roy, N.; Pramanik, H. A. R.; Paul, P. C.; Singh, S. T. *J Fluoresc* **2014**, *24*, 1099.
(139) Yuan, L.; Lin, W.; Yang, Y.; Chen, H. *J. Am. Chem.Soc.* **2012**, *134*, 1200−1211.
(140) Rannulu, N. S.; Rodgers, M. T. *J. Phys. Chem. A* **2012**, *116*, 1319−1332.
(141) Aliaga-Alcalde, N. i.; uez, L. R.; Ferbinteanu, M.; Höfer, P.; Weyhermüller, T. *Inorg. Chem.* **2012**, *51*, 864−873.
(142) Frisch, M. J.; Trucks, G. W.; Schlegel, H. B.; Scuseria, G. E.; Robb, M. A.; Cheeseman, J. R.; Montgomery, J. A.; Vreven, T.; Kudin, K. N.; Burant, J. C.; Millam, J. M.; Iyengar, S. S.; Tomasi, J.; Barone, V.; Mennucci, B.; Cossi, M.; Scalmani, G.; Rega, N.; Petersson, G. A.; Nakatsuji, H.; Hada, M.; Ehara, M.; Toyota, K.; Fukuda, R.; Hasegawa, J.; M.Ishida; Nakajima, T.; Honda, Y.; Kitao, O.; Nakai, H.; Klene, M.; Li, X.; Knox, J. E.; H.P.Hratchian; Cross, J. B.; Bakken, V.; Adamo, C.; Jaramillo, J.; Gomperts, R.; R.E. Stratmann; Yazyev, O.; Austin, A. J.; Cammi, R.; Pomelli, C.; Ochterski, J. W.; Ayala, P. Y.; K.Morokuma; Voth, G. A.; Salvador, P.; Dannenberg, J. J.; Zakrzewski, V. G.; Dapprich, S.; Daniels, A. D.; Strain, M. C.; Farkas, O.; Malick, D. K.; Rabuck, A. D.; Raghavachari, K.; Foresman, J. B.; Ortiz, J. V.; Cui, Q.; Baboul, A. G.; Clifford, S.; Cioslowski, J.; Stefanov, B. B.; Liu, G.; Liashenko, A.; Piskorz, P.; Komaromi, I.; Martin, R. L.; Fox, D. J.; Keith, T.; Laham, A.; Peng, C. Y.; Nanayakkara, A.; Challacombe, M.; Gill, P. M. W.; Johnson, B.; Chen, W.; Wong, M. W.; Gonzalez, C.; Pople, J. A. **2009**.
(143) Walkup, L. L.; Weerasinghe, K. C.; Tao, M.; Zhou, X.; Zhang, M.; Liu, D.; Wang, L. *J. Phys. Chem. C* **2010**, *114*, 19521.
(144) Kim, H. J.; Park, S. Y.; Yoon, S.; Kim, J. S. *Tetrahedron Letters* **2008**, *64* 1294.
(145) Gorelsky, S. I.; Basumallick, L.; Vura-Weis, o.; Sarangi, R.; Hodgson, K. O.; Hedman, B.; Fujisawa, K.; Solomon, E. I. *Inorg. Chem.* **2005**, *44* 4947.
(146) Billing, G. D.; Wang, L. *J. Phys. Chem.* **1992**, *96*, 2572.
(147) Wang, L.; Kalyanaraman, C.; McCoy, A. B. *J. Chem. Phys.* **1999**, *110*, 11221.
(148) Rappoport, Z.; Marek, I. *John Wiley & Sons* **2007**, 107.